Chinese Chemical Letters 35 (2024) 108748

Contents lists available at ScienceDirect

Chinese Chemical Letters

journal homepage: www.elsevier.com/locate/cclet

Highly effective self-assembled porphyrin MOCs nanomaterials for enhanced photodynamic therapy in tumor

Yihao Zhang[a], Yang Jiao[b,*], Xianchao Jia[a], Qiaojia Guo[a], Chunying Duan[b]

[a] School of Chemistry, Dalian University of Technology, Dalian 116024, China
[b] State Key Laboratory of Fine Chemicals, School of Chemistry, Dalian University of Technology, Dalian 116024, China

ARTICLE INFO

Article history:
Received 17 May 2023
Revised 20 June 2023
Accepted 27 June 2023
Available online 28 June 2023

Keywords:
Metal-organic cage
Porphyrin
Photodynamic therapy
Reactive oxygen species
Nanoparticles

ABSTRACT

Porphyrins and their derivatives are excellent photosensitizers in photodynamic therapy (PDT). The modification of porphyrin molecules into metal-organic cages (MOCs) is a viable strategy to improve their bioavailability. In this work, MOC C66 based on porphyrin was synthesised by a one-pot self-assembly method. The three-dimensional structure of the metal-organic cage ameliorated the aggregation and self-quenching of porphyrins and increased the molar absorption coefficient in the visible light region, which enhanced the reactive oxygen species (ROS) yield of porphyrins and effectively improved the efficiency of photodynamic therapy. ROS generation ability tests in solution confirmed the improved reactive oxygen capacity of the cage, which showed greater phototoxicity to HeLa and MCF-7 cells *in vitro*, suggesting a new strategy for future modifications of the simple synthesis of porphyrins as photosensitizers.

Photodynamic therapy (PDT) is an emerging treatment for tumor that depends on the interaction of photosensitizer (PS), light source and oxygen to produce highly toxic reactive oxygen species (ROS) [1,2]. The principle of PDT is that PS absorbs the energy of photons in a specific wavelength and transforms from ground state to excited singlet state (^{1}PS*) and then thrice excited triplet state (^{3}PS*) by inter-systemic crossing (ISC), which generates reactive oxygen species by electron transfer or energy transfer with oxygen molecules, leading to apoptosis or necrosis of tumor cells then results in tumor cell death [3–6]. Compared with traditional treatments such as radiotherapy and chemotherapy, PDT has the advantages of good efficacy, low invasiveness, low systemic toxicity, low drug resistance and high selectivity, enabling it to become a research hotspot in the treatment of various tumors [7–10].

Porphyrins and their derivatives are a classical type of photosensitizers that have been extensively studied because of their widespread occurrence in nature and their excellent photophysical and photochemical properties [11–13]. Porphyrins have a large π-conjugated aromatic structure in their core, a large absorption peak with a large molar extinction coefficient in the visible region and high ROS yields. But π-π interactions between porphyrin molecules can result in aggregation and self-quenching under high concentrations, hindering ROS production. It is necessary to improve the self-quenching of porphyrins in order to enhance their biological activity in PDT [14,15]. The introduction of hydrophilic substituents through covalent linkages to avoid the aggregated self-quenching effect of porphyrins is a common and feasible class of methods [16–19]. It is still a challenge to develop a strategy that can effectively improve the photosensitive properties of porphyrins through a simple preparation process.

The use of photosensitizers in metal-organic cages (MOCs) for biomedical applications has attracted considerable attention in the past few years [20–22]. MOCs are easily functionalized by ligand modification and have a fixed stereospecific conformation that general metal complexes and ligands never provide. The presence of various non-covalent interactions, such as hydrogen bonding, π-π stacking, electrostatic interactions, hydrophobic or hydrophilic effects, gives MOCs excellent flexibility and more efficient application compared to conventional covalently linked complexes, offering great potential in various fields such as molecular identification [23], drug delivery [24], imaging or anti-cancer activity [25] and PDT [26,27]. In addition, discrete MOCs are prepared at the molecular level and tend to be distributed in sizes of a few nanometre. The larger size provides advantages for the MOCs in biology applications, such as promoting enhanced permeation and retention (EPR) effects in tumors to enhance drug uptake and release, which conforms to the ultimate goal of nanomedicine technology [28]. Through the application of metal-organic cages and improvements to porphyrin photosensitizers, incorporating porphyrins as building blocks in metal-organic cages and using them as precur-

* Corresponding author.
E-mail address: jiaoyang@dlut.edu.cn (Y. Jiao).

https://doi.org/10.1016/j.cclet.2023.108748
1001-8417/

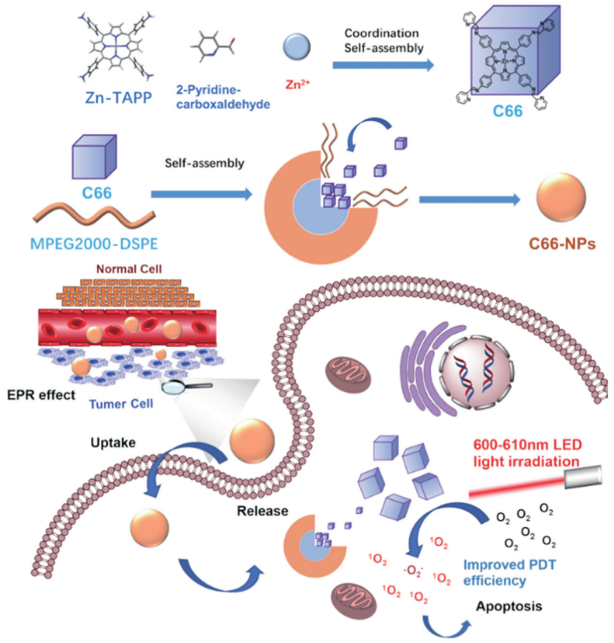

Scheme 1. Preparation, uptake and release of metal-organic cages nanoparticles C66 for PDT in cancer cell followed by *in situ* production of ROS under light emitting diode (LED) light irradiation.

sors for constructing metal-organic cages has tremendous potential to enhance the efficacy of PDT.

In this work, the porphyrin ligand 5,10,15,20-tetra-(4-aminophenyl)porphyrin (TAPP) and ligand Zn-TAPP were synthesized and subsequently self-assembled by a one-pot method to generate a porphyrin-based cubic metal-organic cage C66. Compared with the ligand Zn-TAPP, the porphyrin hexahedral MOCs have improved molar extinction coefficients in the visible region, the potential metal heavy atom effect further enhances the ISC efficiency of the MOCs, the fixed spatial structure inhibits molecular aggregation, resulting in efficient light energy utilization and ROS generation. Characterization of the ability to generate reactive oxygen species in solutions of C66 and Zn-TAPP shows that C66 has a stronger ability to generate singlet oxygen and superoxide anion radicals, enabling it to rapidly provide large amounts of reactive oxygen for other reactions (Scheme 1). More significantly, C66 exhibits extreme photocytotoxicity to HeLa and MCF-7 cells after modification into nanoparticles, while being almost non-toxic under the dark conditions. Synthesizing and modifying a porphyrin-based metal-organic cage opens up a new strategy for PDT applications *in vitro* biological systems.

The ligands 5,10,15,20-tetrakis(4-nitrophenyl)porphyrin (TNPP), TAPP, and Zn-TAPP were prepared according to the previous literatures (Figs. 1a and b and Figs. S1–S5 in Supporting information) [29–31]. Zn-TAPP was ultimately obtained and used as a self-assembled ligand for the next reaction in the formation of C66 MOC. The reaction of Zn-TAPP (6 equiv.) with 2-pyridinecarboxaldehyde (24 equiv.) was then carried out in the presence of $Zn(OTf)_2$ (8 equiv.) to form a cubic complex whose structure is $Zn_8L_6(OTf)_{16}$ [32,33].

The corresponding hydrogen signals in Zn-TAPP and C66-MOC were first analyzed by proton nuclear magnetic resonance (^{1}H NMR) spectroscopy after preparation. The downfield shift of the whole signals probably caused by the coordination of ligand to metal atom. The disappearance of the hydrogen signal of the porphyrin amino group (δ 5.47) and the appearance of the hydrogen signal at δ 9.05 correspond to the reaction of amino group with 2-pyridinecarboxaldehyde to form the imine structure (Fig.

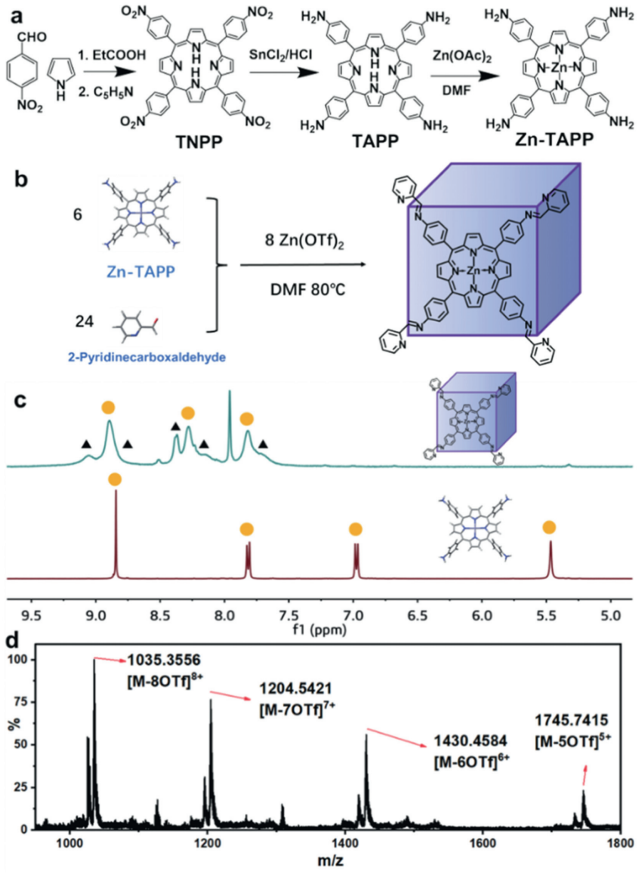

Fig. 1. (a) Synthetic route to the ligand Zn-TAPP. (b) Self-assembly route of the metal-organic cage C66. (c) Comparison of the ^{1}H NMR spectra of C66 and Zn-TAPP. (d) ESI-MS spectrum of C66 MOC.

1c). Moreover, the hydrogen signal of the imine has a fixed proportional relationship with the hydrogen signals of the pyrrole and benzene ring units corresponding to Zn-TAPP, confirming the formation of a highly symmetrical metal-organic cage in actuality.

The structure was further characterized by electrospray ionization mass spectrometry of C66. The mass spectra showing that signals were appeared at *m/z* of 1035.3556, 1204.5421, 1430.4584 and 1745.7415 (Fig. 1d and Table S1 in Supporting information), corresponding to $[M-8OTf]^{8+}$ $[M-7OTf]^{7+}$ $[M-6OTf]^{6+}$ and $[M-5OTf]^{5+}$. A simple comparison with simulations based on natural isotopic abundances shows that these peaks can correspond well to their corresponding measured values of $[Zn_8L_6(OTf)_n]^{(16-n)+}$ ($n=8$–11) (Fig. S6 in Supporting information). The analysis of starting material ratio in experiment, hydrogen signal proportion in ^{1}H NMR and *m/z* values in electrospray ionization mass spectrometry (ESI-MS) spectra shows that the MOC was a structure composed of Zn_8L_6 $(OTf)_{16}$. Based on similar structures that have been prepared [34,35], the cubic configuration of the metal cage was ultimately determined. In this cubic structure, Zn-porphyrins act as the surface of MOCs, eight zinc atoms are occupying each of the eight vertices, which forms a coordination pattern of $Zn(N\text{-}N)_3$ through sp^3d^2 hybridization with six nitrogen atoms from each of the three ligands. The above data confirmed the formation of $Zn_8L_6(OTf)_{16}$ metal-organic cages.

After determining the correct structure of the metal-organic cages, the absorption spectra and fluorescence emission spectra of ligand Zn-TAPP and MOC C66 in different common solvents were recorded using an ultraviolet visible (UV–vis) spectrophotometer and a fluorescence spectrometer (Figs. 2a and b). The absorption

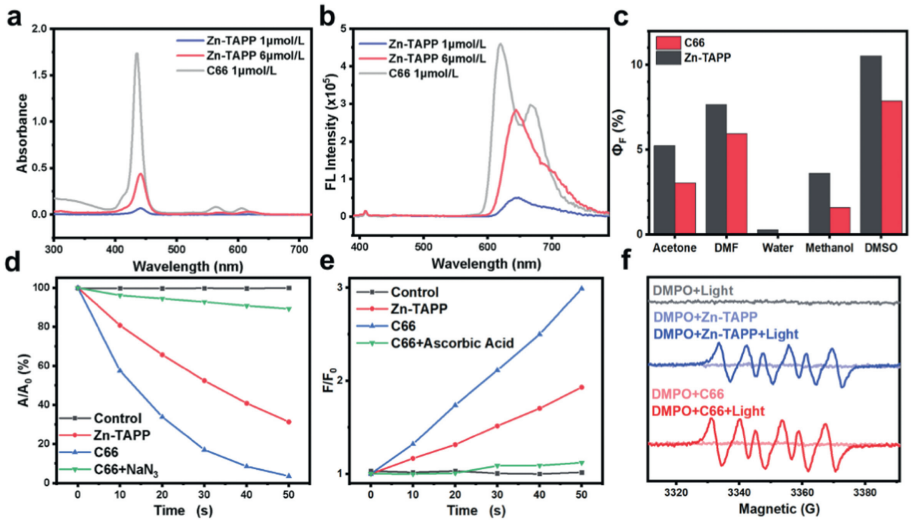

Fig. 2. (a, b) The absorption and fluorescence spectra of Zn-TAPP(1 μmol/L), Zn-TAPP (6 μmol/L) and C66 (1 μmol/L) in DMSO. (c) Fluorescence quantum yields of Zn-TAPP and C66 in different solvents. (d) Plots of ΔAbs (A/A_0) for DPBF at 418 nm upon LED light irradiation (600–610 nm, 20 mW/cm^2) for different time intervals in the presence of Zn-TAPP or C66. (e) Plots of F/F_0 for DHR123 at 542 nm upon LED light irradiation (600–610 nm, 20 mW/cm^2) for different time intervals in the presence of Zn-TAPP or C66. (f) ESR spectra to detect $\cdot O_2^-$ generated by Zn-TAPP (36 μmol/L) or C66 (6 μmol/L) under illumination, using DMPO (100 mmol/L) as a spin trap.

peaks of Zn-TAPP and MOCs in different solvents were concentrated around 415, 580 and 610 nm, while the emission peaks were concentrated around 620 nm, with slight variations depending on the solvent. Both the ligand and the metal cage showed intense red fluorescence when the excitation light wavelength was chosen to be 365 nm, with a distinct set of emission peaks near 650 nm corresponding to the porphyrin core. Analysis of the UV–vis absorption and fluorescence emission spectra of Zn-TAPP (6 equiv.) and C66 (1 equiv.) in dimethyl sulfoxide (DMSO) showed that the molar extinction coefficient of C66 (1 equiv.) at the absorption peak was higher than that 6 equiv. Zn-TAPP, while the fluorescence intensities were similar. Subsequently, the fluorescence quantum yield (Φ_F) of both ligands and metal cages was measured using Rhodamine B (Φ_F = 31% in water) as a standard (Fig. 2c, Fig. S7, Tables S2 and S3 in Supporting information) [36,37]. The reduced fluorescence quantum yield of the metal cage compared to the porphyrin ligand indicates that the energy conversion *via* the fluorescence emission pathway has been partially suppressed and more energy has the opportunity to enter from $^1PS^*$ to $^3PS^*$ through ISC process, promoting the production of reactive oxygen species [38], which means that the porphyrin ligand could be successfully improved in its photosensitive properties after modification into the metal-organic cage.

Singlet oxygen, a common reactive oxygen species, plays a major role in apoptosis in PDT [39]. To determine the ability of Zn-TAPP and C66 to release $^1O_2$ under red light excitation, 1,3-diphenylisobenzofuran (DPBF) was used as an indicator to measure $^1O_2$ [40]. In the presence of singlet oxygen, DPBF can be oxidized to endoperoxides, which further decompose to the low-fluorescence 1,2-dibenzoylbenzene. The performance of the photosensitizer in producing singlet oxygen can be deduced by observing the reduction of the absorption peak of DPBF at 418 nm. After irradiation of the porphyrin Zn-TAPP and C66 in DMSO solution for 50 s with a 600–610 nm LED lamp, the absorption peak of DPBF at 418 nm was reduced by 67% for 6 equiv. of Zn-TAPP, indicating that porphyrins are a very good class of singlet oxygen donors. By comparison, 1 equiv. of C66 showed a more intense DPBF decomposition efficiency (a decrease of almost 100%), indicating that more $^1O_2$ was produced (Fig. 2d and Fig. S8 in Supporting information). Conversely, the addition of the singlet oxygen quencher NaN_3 strongly inhibited the $^1O_2$ production capacity of C66, partially confirming the ability of the cage to specifically and efficiently produce singlet oxygen [41].

Interestingly, while determining other possible ROS, we also discovered its ability to generate superoxide radicals, and the presence of superoxide anion radicals provides C66 with another novel PDT type I process, which allows C66 to still produce a large amount of reactive oxygen species and cause cell death under possible hypoxic conditions in tumor tissue [42,43]. To determine whether ligands and C66 are able to release $\cdot O_2^-$ under red light excitation, dihydrorhodamine 123 (DHR123) was used as an indicator for the determination of $\cdot O_2^-$ [44,45]. In the presence of $\cdot O_2^-$, DHR123 can be oxidized to rhodamine 123 with strong green fluorescence, and the ability of the photosensitizer to produce $\cdot O_2^-$ can be confirmed by observing the magnitude of the increase in fluorescence generation peak at 540 nm in DMSO. After irradiation of the porphyrin ligand or C66 in DMSO solution with 600–610 nm LEDs for 50 s, DHR123 produced nearly a two-fold increase in fluorescence at 540 nm for 6 equiv. of Zn-TAPP, indicating the ability of the porphyrin ligand to produce $\cdot O_2^-$, while C66 showed better $\cdot O_2^-$ production than the porphyrin ligand (3-fold fluorescence enhancement) (Fig. 2e and Fig. S9 in Supporting information). Further addition of the $\cdot O_2^-$ quencher ascorbic acid drastically inhibited the $\cdot O_2^-$ production capacity of C66, while confirming the $\cdot O_2^-$ production capacity of C66 MOC [46]. Electron spin resonance (ESR) spectroscopy was employed to further confirm the $\cdot O_2^-$ generation by sensitization of C66. 5,5-Dimethyl-1-pyrroline-*N*-oxide (DMPO) was used as a spin-trap agent for $\cdot O_2^-$. Upon light-irradiation of the aerated solution of C66 and DMPO, a characteristic paramagnetic adduct was observed and matched with the $\cdot O_2^-$ signal thereby confirming the $\cdot O_2^-$ production (Fig. 2f). It is concluded that the photophysical and photochemical properties of the porphyrins were successfully improved by metal-organic cage modification, which enhanced the reactive oxygen generation capacity of the porphyrin photosensitive molecules.

Although MOCs have improved photosensitiser performance compared to the original Zn-TAPP, they still exhibited unsatisfactory water solubility, which hinders their application in living organisms. Further modification of MOCs into special structures with excellent water solubility is paramount to promote their application in cancer therapy. Here, a nanoparticle with high water solubility and biomass application was prepared by nanoprecipita-

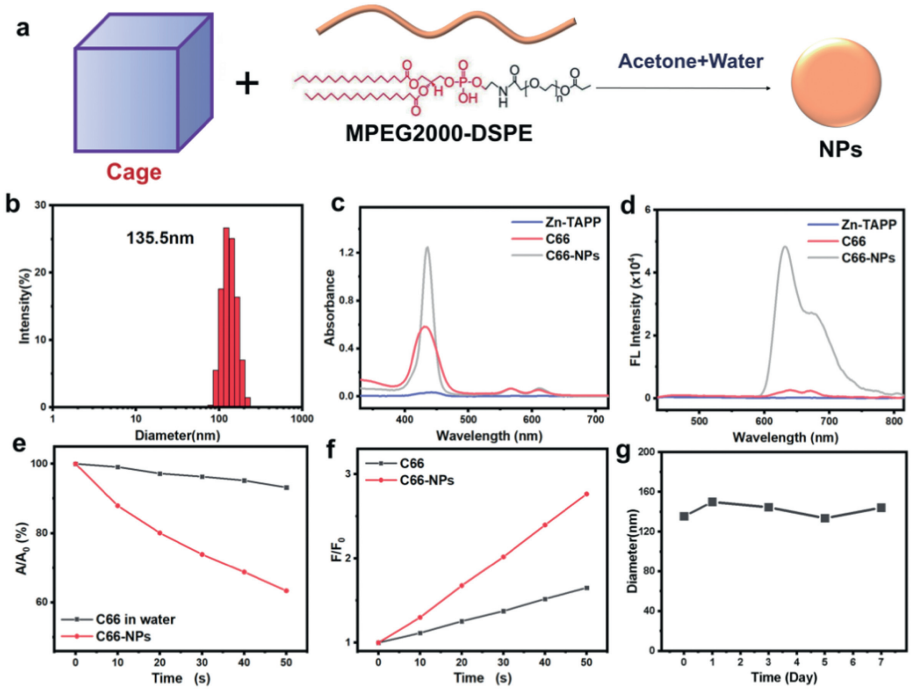

Fig. 3. (a) The scheme of the preparation of supramolecular PS nanoparticles (C66-NPs). (b) DLS result of C66-NPs. (c, d) The absorption and fluorescence spectra of Zn-TAPP, C66 and C66-NPs (1 μmol/L) in water. (e, f) Plots of ΔAbs (A/A_0) and F/F_0 for DPBF and DHR123 to characterize the ROS generation upon LED light irradiation (600–610 nm, 20 mW/cm^2) for different time intervals in the presence of water solution of C66 or C66-NPs. (g) Diameter change of nanoparticles C66-NPs within one week.

tion using the amphiphilic molecule methyl polyethylene glycol-distearoyl phosphoethanolamine (MPEG-DSPE) to encapsulate and cover the MOCs [47]. An aqueous solution of the nanoparticles was prepared by rapidly injecting an acetone solution of cage C66 into an aqueous solution of MPEG-DSPE and then evaporating any residual acetone (Fig. 3a). The nanoparticles were then filtered through a 0.22 μm filter membrane, which was obtained by dynamic light scattering (DLS) analysis with a diameter distribution of around 130 nm (Fig. 3b).

A facile test of photophysical properties and reactive oxygen generation capacity was carried out after the successful preparation of C66 nanoparticles. The UV–vis absorption and fluorescence emission of the MOCs in water were enhanced after modification to nanoparticles, which can be attributed to the more superior water solubility (Figs. 3c and d). In addition, a comparison of the $^1O_2$ and $\cdot O_2^-$ production capacities of C66 and its nanoparticles C66-NPs in aqueous solution also confirmed that the nanoparticles C66-NPs are competent for the efficient generation of reactive oxygen species in aqueous solution as well as in the cellular environment (Figs. 3e and f). While possessing superior photosensitizer performance, C66-NPs also exhibit good stability. After placing the C66-NPs solution for one week, the approximate particle size and the absorption spectrum of C66-NPs had almost no change, which laid the foundation for the storage and application of nanoparticles (Fig. 3g and Fig. S10 in Supporting information).

Inspired by the efficient production of reactive oxygen species under red light irradiation by C66 and nanoparticles C66-NPS, we started to study their effect *in vitro* for PDT with laser confocal scanning microscopy (CLSM). At first, the cellular uptake capacity of C66-NPs was characterised. The diameter of nanoparticles is about 140 nm, for microvascular endothelium with dense gaps and complete structure in normal tissues, nanoparticles do not easily penetrate the vessel wall. In contrast, solid tumor tissue is characterised by abundant blood vessels, large vessel wall gaps and poor structural integrity, which allows C66 nanoparticles to have EPR at the tumor site, making them easily phagocytosed into the cytoplasm by cancer cells, promoting selective distribution in tumor tissue and improving drug efficacy and reducing systemic side effects. As expected, HeLa cells showed red fluorescence in the cytoplasm after uptake of C66-NPs when Zn-TAPP, C66 and C66-NPs were incubated with HeLa cells for 4.0 h respectively, in contrast to unmodified nanoparticles where Zn-TAPP and MOCs were more difficult to take up into the cells and therefore did not fluoresce significantly (Fig. S11 in Supporting information), further confirming the good cellular uptake process.

To assess the feasibility of nanoparticles in cancer therapy, 3-(4′,5′-dimethylthiazol-2′-yl)-2,5-diphenyl tetrazolium bromide (MTT) was used to further evaluate the feasibility of nanoparticles in cancer therapy at concentrations ranging from 0 to 10 μmol/L [48]. It is noteworthy that C66-NPs exhibited relatively low dark cytotoxicity at this concentration range (Fig. 4a), which avoids the unwanted systemic toxicity associated with PDT. C66 NPs induced *in situ* production of the potent cytotoxic $^1O_2/\cdot O_2^-$ under light conditions, with half-inhibitory concentrations in range of 0.5–1 μmol/L, predicting excellent therapeutic effects (Fig. 4b). Then, we characterised the ability of intracellular ROS production and detected changes in intracellular ROS during PDT using the ROS probe 2′,7′-dichlorodihydrofluorescein diacetate (DCFH-DA) [43]. Bright green fluorescence was observed in C66-NPs-treated HeLa cells by CLSM after light irradiation, indicating effective ROS production (Fig. 4c). To verify the phototoxicity of C66-NPs in cancer cells, the cells were further stained with calcein-AM and propidium iodide (PI) to detect the effect of C66-NPs on tumor cells through oxidative damage [49]. C66-NPs-treated HeLa cells showed almost no signals in green channel and significant signals in red channel after illumination, indicating almost complete HeLa cell death. On the contrary, C66-NPs treated cells showed fluorescence only in green channel in absence of light, indicating negligible cell death, while the majority of cells incubated with Zn-TAPP and C66 remained alive, corresponding to poorer cellular uptake (Fig. 4d). Then, an Annexin V-fluorescein isothiocyanate (FITC)/PI apoptosis detection kit was used to study apoptotic cells, and the

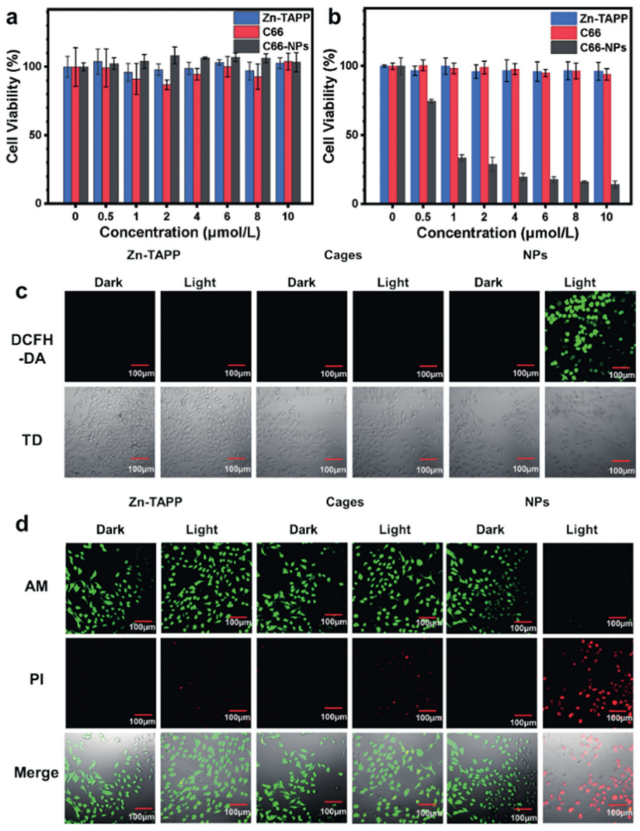

Fig. 4. (a, b) Cell viability of HeLa cells subjected to a range of C66-NPS in the absence and presence of LED light-irradiation (600–610 nm, 20 mW/cm^2). (c) Detection of ROS in HeLa cells under normoxia conditions with DCFH-DA. (d) CLSM images of calcein AM/PI-stained HeLa cells under normoxia conditions. Scale bar: 100 μm.

experimental results showed that C66-NPs can effectively induce tumor cell apoptosis through PDT to achieve the therapeutic goal (Fig. S12 in Supporting information). In addition, when C66-NPs are applied to other cancer cell lines, such as MCF-7 cell lines, they still have good PDT effects, which can cause similar reactive oxygen species production ability and cell phototoxicity, and have good results in a wide range of tumor cell PDT (Fig. S13 in Supporting information). The construction of C66 and modification of C66-NPs not only significantly improved the water-soluble and light-sensitive properties of porphyrin, but also provided a highly efficient cellular uptake process. After rapid and accurate enrichment in tumor tissue, C66 effectively produces large amounts of highly cytotoxic ROS under irradiation conditions, resulting in apoptosis of tumor cells. The excellent performance of C66 NPs provides a viable strategy for simple and efficient modification of porphyrin-based photosensitizers.

In summary, the C66 MOCs based on porphyrin core units have been synthesized to improve the efficacy of PDT. The common porphyrin derivative ligand was modified into the cage as the surface of the MOCs, while the introduction of zinc atoms provided the attachment sites for the MOCs to self-assemble into cubic cages. The cage has a higher molar extinction coefficient than the original ligand, increasing the extent to which the porphyrin is available for visible light; the design of the cage provides a fixed spacing for the porphyrin and inhibits self-aggregation. C66 nanoparticles were prepared to effectively increase water solubility with a certain efficiency of reactive oxygen species generation. The nanoparticles were able to induce apoptosis of tumor cells effectively by PDT after internalization by cancer cells. This work provides new directions and ideas for simple modifications of porphyrins for application in biological systems, which can be used as photosensitizers for PDT of excellent performance.

Declaration of competing interest

The authors declare that they have no known competing financial interests or personal relationships that could have appeared to influence the work reported in this paper.

Acknowledgment

This work was supported by the National Natural Science Foundation of China (Nos. 21977015 and 21820102001).

Supplementary materials

Supplementary material associated with this article can be found, in the online version, at doi:10.1016/j.cclet.2023.108748.

References

[1] L. Shi, F. Hu, Y. Duan, et al., ACS Nano 14 (2020) 2183–2190.
[2] M. Li, Y. Xu, X. Peng, J.S. Kim, Acc. Chem. Res. 55 (2022) 3253–3264.
[3] X. Li, N. Kwon, T. Guo, Z. Liu, J. Yoon, Angew. Chem. 130 (2018) 11694–11704.
[4] X. Li, S. Lee, J. Yoon, Chem. Soc. Rev. 47 (2018) 1174.
[5] Z. Zhuang, J. Dai, M. Yu, et al., Chem. Sci. 11 (2020) 3405–3417.
[6] S. Li, Q. Zou, Y. Li, et al., J. Am. Chem. Soc. 140 (2018) 10794–10802.
[7] S.R.G. Fernandes, T. Mohajershojai, S. Lundsten, et al., J. Photoch. Photobio. B 243 (2023) 112716.
[8] A. Amirjani, P. Shokrani, S.A. Sharif, et al., J. Mater. Chem. B 11 (2023) 3537.
[9] B. Yuan, H. Wu, H. Wang, et al., Angew. Chem. Int. Ed. 60 (2021) 706–710.
[10] J. Du, T. Shi, S. Long, et al., Coord. Chem. Rev. 427 (2021) 213604.
[11] M. Lan, S. Zhao, W. Liu, et al., Adv. Healthc. Mater. 8 (2019) 1900132.
[12] B.M. Amos-Tautua, S.P. Songca, O.S. Oluwafemi, Molecules 24 (2019) 2456.
[13] F. Yang, Q. Ji, R. Liao, et al., Chin. Chem. Lett. 33 (2022) 1927–1932.
[14] M. Daurat, C. Nguyen, S.D. Gil, et al., Biomater. Sci. 8 (2020) 3678–3684.
[15] J. Longevial, K.E. Cheikh, D. Aggad, et al., Chem. Eur. J. 23 (2017) 14017–14026.
[16] Z. Lv, L. Zou, H. Wei, et al., ACS Appl. Mater. Interfaces 10 (2018) 19523–19533.
[17] P. Gao, M. Wang, Y. Chen, et al., Chem. Sci. 11 (2020) 6882.
[18] Q. Wang, Q. Chen, G. Jiang, et al., Chin. Chem. Lett. 30 (2019) 1965–1968.
[19] Z. Meng, B. Shan, L. Zhang, et al., Chin. Chem. Lett. 27 (2016) 623–626.
[20] Y. Yao, R. Zhao, Y. Shi, et al., Chem. Commun. 54 (2018) 8068.
[21] G. Li, X. Zhang, W. Zhao, et al., ACS Appl. Mater. Interfaces 12 (2020) 20180–20190.
[22] C. Wang, J. Shang, L. Tian, et al., Chin. Chem. Lett. 32 (2021) 4006–4010.
[23] T. Feng, X. Li, J. Wu, C. He, C. Duan, Chin. Chem. Lett. 31 (2020) 95–98.
[24] Z. Yue, H. Wang, D.J. Bowers, et al., Dalton Trans. 47 (2018) 670.
[25] G. Gupta, A. Das, K.C. Park, et al., Inorg. Chem. 56 (2017) 4615–4621.
[26] P.C. Purba, M. Maity, S. Bhattacharyya, P.S. Mukherjee, Angew. Chem. Int. Ed. 60 (2021) 14109–14116.
[27] C. Lia, Y. Wang, Y. Lu, et al., Chin. Chem. Lett. 31 (2020) 1183–1187.
[28] Y. Sun, H. Zhang, G. Lu, et al., Chin. Chem. Lett. 34 (2023) 107817.
[29] D. Yadav, A. Kumar, J.Y. Kim, N. Park, J. Baeg, J. Mater. Chem. A 9 (2021) 9573.
[30] G. Prabhavathi, R. Yamuna, A.C. Jafer, J. Organomet. Chem. 861 (2018) 219e229.
[31] L. Li, H. Guo, L. Yang, et al., Inorg. Chem. 59 (2020) 2636–2640.
[32] E.G. Percástegui, J. Mosquera, J.R. Nitschke, Angew. Chem. Int. Ed. 56 (2017) 9136–9140.
[33] E.G. Percástegui, T.K. Ronson, J.R. Nitschke, Chem. Rev. 120 (2020) 13480–13544.
[34] N. Struch, C. Bannwarth, T.K. Ronson, Angew. Chem. Int. Ed. 56 (2017) 4930–4935.
[35] M. Otte, P.F. Kuijpers, O. Troeppner, Chem. Eur. J. 20 (2014) 4880–4884.
[36] J. Zhou, Y. Zhang, G. Yu, et al., J. Am. Chem. Soc. 140 (2018) 7730–7736.
[37] A.T.R. Williams, S.A. Winfield, J.N. Miller, Analyst 108 (1983) 1067–1071.
[38] C. Chen, X. Ni, H. Tian, et al., Angew. Chem. Int. Ed. 59 (2020) 10008–10012.
[39] E. Pang, S. Zhao, B. Wang, et al., Coord. Chem. Rev. 472 (2022) 214780.
[40] H. Huang, D. Huang, M. Li, et al., Dyes Pigments 177 (2020) 108284.
[41] K. Teng, L. Niu, Q. Yang, Chem. Sci. 13 (2022) 5951.
[42] X. Li, D. Lee, J. Huang, J. Yoon, Angew. Chem. 130 (2018) 10033–10038.
[43] Y. Xiao, W. Chen, J. Chen, et al., ACS Appl. Mater. Interfaces 14 (2022) 5112–5121.
[44] Y. Ding, Z. Wang, Z. Zhang, et al., Nano Res. 15 (2022) 7304–7312.
[45] K. Teng, W. Chen, L. Niu, et al., Angew. Chem. Int. Ed. 60 (2021) 19912–19920.
[46] M. Li, J. Xia, R. Tian, et al., J. Am. Chem. Soc. 140 (2018) 14851–14859.
[47] G. Yu, T.R. Cook, Y. Li, et al., Peoc. Natl. Acad. Sci. U. S. A. 113 (2016) 13720–13725.
[48] Y. Qin, L. Chen, F. Dong, et al., J. Am. Chem. Soc. 141 (2019) 8943–8950.
[49] X. Wu, M. Xu, S. Wang, et al., Dalton Trans. 51 (2022) 2296.